Preparation, characterization and electrocatalytic activity of transition metal @ platinum on carbon support for alkaline ethanol electro-oxidation

R. M. Abdel Hameed[1] · Amani E. Fetohi[2] · K. M. El-Khatib[2] · R. S. Amin[2]

Abstract

The effect of adding a transition metal (M) to the core structure of M@Pt/C electrocatalyst on its electrocatalytic activity towards ethanol oxidation reaction in alkaline medium was studied. Copper or nickel or cobalt was reduced on Vulcan XC-72R carbon black surface using sodium borohydride followed by introducing platinum ions in the shell structure. The crystalline nature and the electrocatalyst morphology were investigated using XRD and TEM analysis techniques. Cyclic voltammetry, electrochemical impedance spectroscopy and chronoamperometry were applied to evaluate the electrocatalytic characteristics of prepared nanocatalysts during alcohol electro-oxidation. The electrocatalytic activity showed an ascending behavior as Cu@Pt/C < Ni@Pt/C ~ Co@Pt/C. The exchange current density at Co@Pt/C was 11.28 folds higher than that at Pt/C. Lowered charge transfer resistance values were also measured at all M@Pt/C electrocatalysts when related to that at Pt/C. The enhanced performance of core–shell structured M@Pt/C electrocatalysts suggests the application of this developed method for fabricating efficient multimetallic nanocomposites for fuel cells.

Keywords Electrocatalytic activity · Core–shell structure · Electrocatalyst · Alkaline medium · Platinum nanoparticles

1 Introduction

A great interest has been directed to the electrocatalytic oxidation of alcohols as a result of their potential applications in the electrosynthesis of organic compounds and energy conversion technology [1–3]. Direct ethanol fuel cells have shown many advantages when compared to those based on methanol and formic acid [4]. Ethanol could be easily formed during the fermentation of agricultural products or other biomass with low toxicity and high theoretical mass energy density [5–7]. However, it is difficult to break C–C bond in ethanol to form CO_2 and H_2O which may retard the complete oxidation of ethanol [8, 9]. This could be overcome by preparing an efficient anode material such as Pt and Pt-based electrocatalysts.

However, the commercial application of direct alcohol fuel cells is hindered because of the increased price of platinum metal. Therefore, many research groups have studied the possibility of increasing the catalytic activity and stability of Pt-based electrocatalysts by employing reduced amounts of noble metals [10]. This aim could be achieved by combining platinum with cheap transition metals such as nickel, cobalt or copper. They exhibit good electrochemical activity and stability to improve the electrocatalytic performance of Pt-based composites when introduced in appropriate ratios. XRD charts displayed a decreased lattice constant of Pt diffraction peaks in PtNi/C catalyst, synthesized via the polyol process, when compared to Pt/C to indicate the formation of a partial PtNi alloy. The electronic structure of Pt in Pt_3Ni/C electrocatalyst has been modified when nickel atoms were introduced, as proved by density functional theory studies, resulting in weak CO adsorption energy which in turn increased the electrocatalyst activity towards methanol oxidation in alkaline medium [11]. Nanoparticles of platinum–nickel supported on titanium surface catalysts by the galvanic displacement showed a higher catalytic efficiency

✉ R. M. Abdel Hameed
   randa311eg@yahoo.com

✉ Amani E. Fetohi
   amaniebaid@yahoo.com

1 Chemistry Department, Faculty of Science, Cairo University, Giza, Egypt

2 Chemical Engineering Department, National Research Center, Dokki, Giza, Egypt

towards borohydride, ethanol and methanol oxidation reactions in comparison with that of pure Pt [12]. Ethanol oxidation peak at $PtNi_3$/MWCNTs electrocatalyst exhibited a negative shift of the onset potential value by 190 mV when related to that at Pt/MWCNTs with an enhanced oxidation peak current density by about 2.5 times [13]. Co@Pt/MWCNTs electrocatalyst displayed 3.36 times higher methanol oxidation mass activity than that at Pt/MWCNTs [14]. The highly ranked stability and activity of Pt/CoSi-graphene for methanol oxidation was attributed to the electron donation of CoSi to Pt [15]. Sheng et al. [16] have prepared platinum–cobalt ($Pt_xCo_{1−x}$, x = 0.70, 0.55) alloy nanoparticles via the chemical reduction route by using a support of carbon Vulcan XC-72. They showed good electrochemical sensing for glucose with linear oxidation current density increase in glucose concentration ranging from 0.10 to 14.20 mM with an elevated sensitivity of 73.60 $\mu A\ mM^{-1}\ cm^{-2}$. Cu@Pt–Ru core–shell supported electrocatalysts exhibited highly ranked catalytic activity for electro-oxidation of ethanol and methanol when related to commercial Pt–Ru/C electrocatalyst with higher Pt loading [17]. Sarkar et al. [18] and Zhu et al. [19] have synthesized a series of Pt–Cu nanoparticles supported on carbon with core–shell structure using chemical reduction and subsequent galvanic replacement methods. The electronic modification of Pt shell with inner Pt–Cu core could rationalize the enhanced electrocatalytic activity for these electrocatalysts towards oxygen reduction reaction. A series of ternary PtAuCu nanoparticles supported on carbon was fabricated by adding variable copper amounts with activating the electrocatalyst surface through an electrochemical route. Activated $Pt_{10}Au_{10}Cu_{80}$/C exhibited superior catalytic activity when oxidizing small organic molecule fuels [20].

Core–shell design has been adopted in nanocatalyst structure by coating a layer of noble metal on another cheap one. This particular structure resulted in improving the catalytic performance of fabricated nanocomposites with reducing their cost [21, 22]. In this work, different M@Pt/C electrocatalysts were prepared with a core–shell architecture, where M = Cu, Ni or Co. The effect of varying the core metal on the electrocatalytic activity of synthesized electrocatalyst towards ethanol oxidation in alkaline medium was investigated. Their crystalline structure and morphology were also studied using XRD and TEM analyses, respectively.

2 Materials and methods

2.1 Chemicals

Vulcan XC-72R carbon black was purchased from Cabot Corp., USA with a specific surface area (BET) of 240 $m^2\ g^{-1}$ and an average particle size of 40 nm. Nafion (perfluorosulphonic acid-PTFE copolymer, 5 wt% solution) and

$H_2PtCl_6\cdot 6H_2O$ were obtained from Sigma-Aldrich, Germany. Other chemicals including $CoCl_2\cdot 6H_2O$, $NiCl_2\cdot 6H_2O$, $CuCl_2\cdot 2H_2O$, $NaBH_4$, ethanol and NaOH were of analytical grade and did not be subjected to purification before use. Solutions were prepared and electrodes were washed using double distilled water.

2.2 Preparation of different M@Pt/C electrocatalysts

Different M@Pt electrocatalysts were supported on Vulcan XC-72R carbon black using $NaBH_4$ as a reducing agent. A calculated amount of metal precursor salt ($CoCl_2\cdot 6H_2O$, $NiCl_2\cdot 6H_2O$ or $CuCl_2\cdot 2H_2O$) was dissolved in the least amount of double distilled water. It was then added drop by drop to $NaBH_4$ solution. The added weight of $NaBH_4$ was calculated such that the molar ratio of M to $NaBH_4$ was 1:15. The total metal loading was kept at 30 wt%. The mixture of metal precursor salt and sodium borohydride was continuously stirred for 30 min. An adequate weight of $H_2PtCl_6\cdot 6H_2O$ was then added and the reduction step was completed using another amount of $NaBH_4$ with constant stirring for another 30 min. Vulcan XC-72R carbon black was then ultrasonically mixed with the above mixture for 30 min, followed by stirring for 3 h. Finally, M@Pt/C electrocatalyst powders were filtered, washed at least for six times and dried at 80 °C for 6 h. Pt/C was prepared using a similar procedure for comparison purposes.

2.3 Physical characterization of prepared electrocatalysts

The crystalline structure of different electrocatalysts powder was studied using X-ray diffraction. A Rigaku-D/MAX-PC 2500 X-ray diffractometer equipped with Ni-filtered Cu K_α as the radiation source was used. The tube current was 40 mA with a voltage of 40 kV. For preparing the electrocatalysts powder during XRD measurement, a glass slide was used to fix the sample powder which was then dried in vacuum overnight. XRD patterns were scanned at 2θ values ranging between 10° and 80°. Transmission electron microscopy was applied to investigate the electrocatalysts morphology and their particle size using JEOL-JEM 2010 transmission electron microscope. Its accelerating voltage was adjusted at 160 kV. The electrocatalyst powders were suspended in a mixture of double distilled water and isopropyl alcohol and sonicated for 30 min in ultra8050-H Clifton. Copper grids coated with carbon film were employed to carry a drop of the electrocatalysts suspension. They were left to dry in the air before measurement. The size of Pt nanoparticles was estimated using Gatan program. SEM model Quanta 250 FEG (field emission gun) was also employed to determine the chemical constituents of Co@

Pt/C electrocatalyst through an attached EDX unit. The mapping images of different elements in this sample were also scanned.

2.4 Electrode fabrication and electrochemical measurements

Electrochemical measurements were conducted using an electrochemical cell connected to Gamry potentiostat. A standard 3-electrodes cell was built up with a glassy carbon electrode coated with the synthesized electrocatalyst powder as the working electrode, Pt wire as the auxiliary electrode and Hg/HgO/1 M NaOH (MMO) as the reference electrode. To prepare the catalyst ink, 10 mg M@Pt/C powder was dispersed in 5 ml isopropyl alcohol and sonicated for 5 min. 50 μl of this suspension was then spread out at the glassy carbon surface and fixed by adding 0.1 ml Nafion solution. It was then dried in the air and stored overnight in a desiccator before use. The electrocatalyst loading on carbon surface was 0.6 mg cm^{-2}. Cyclic voltammetry, chronoamperometry and electrochemical impedance spectroscopy were employed to study the electrochemical activity of differently prepared electrocatalysts. 0.5 M NaOH solution was used as the supporting electrolyte with adding different concentrations of ethanol. In cyclic voltammetry measurements, the studied potential range was extended from −700 to +400 mV at a scan rate of 10 mV s^{-1}. On the other hand, the electrochemical impedance spectroscopic study was operated at a constant dc potential value of −450 mV with ac voltage amplitude of 10 mV and the frequency range was 10,000–0.1 Hz. The working electrode was immersed before each experiment in the test solution for 300 s at the chosen potential value. A complex non-linear least squares (CNLS) circuit fitting software was used to theoretically fit the obtained data according to the proposed equivalent circuit models. All electrochemical measurements were carried out in aerated electrolytes at room temperature of 30 °C ± 0.2.

3 Results and discussion

XRD patterns of Pt/C and different M@Pt/C electrocatalysts were shown in Fig. 1a. The graphite structure of carbon support was detected from a broad peak at 2θ values ranging between 24° and 25°. All charts of prepared electrocatalysts showed the diffraction planes of platinum; namely: Pt(111), Pt(200) and Pt(220). However, their 2θ and d values were dependent of the examined electrocatalyst as indicated in Table 1. This could be also clarified by magnifying the positions of these three diffraction planes in Fig. 1b [Pt(111)], Fig. 1c [Pt(200)] and Fig. 1d [Pt(220)]. A positive shift of these diffraction lines was measured for the electrocatalysts containing transition metals when compared to those in Pt/C.
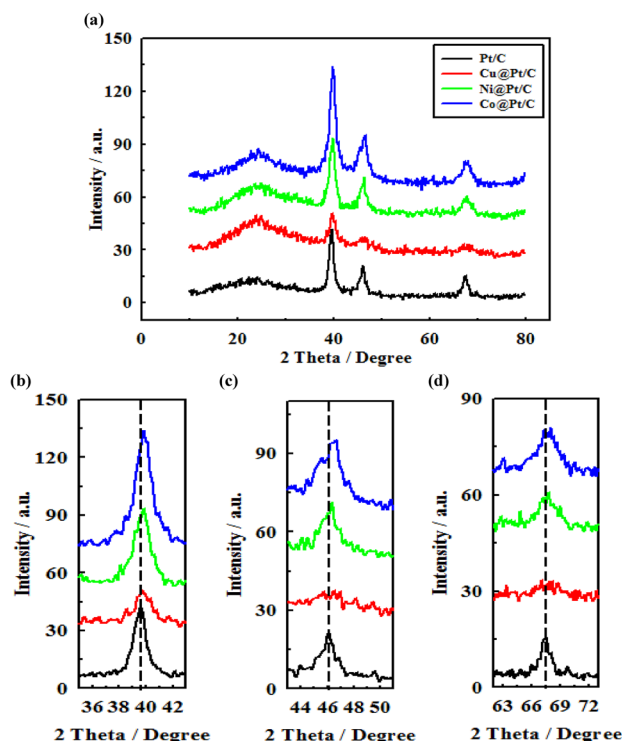
Fig. 1 **a** XRD patterns of Pt/C, Cu@Pt/C, Ni@Pt/C and Co@Pt/C electrocatalysts. Magnifications of the diffraction lines of Pt(111), Pt(200) and Pt(220) were shown in **b, c** and **d**, respectively

The recorded decrease in lattice distance values could reflect the contraction of platinum crystal after incorporating transition metals in the fabricated electrocatalysts. No defined diffraction lines were detected for copper or nickel or cobalt in their respective XRD patterns. This may be attributed to the insertion of these metals inside the platinum lattice [23].
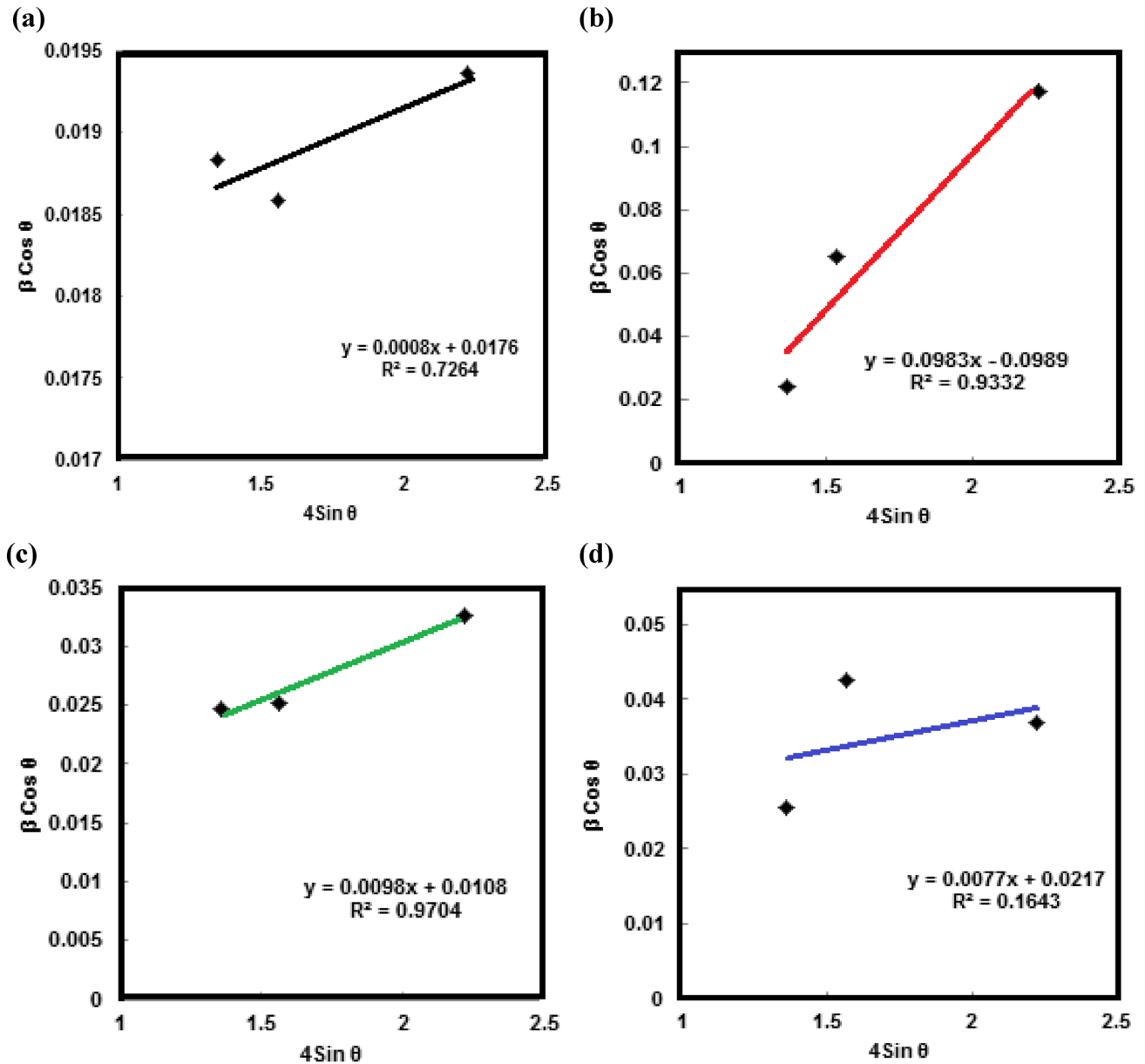
The reactivity of different prepared electrocatalysts mainly depends on their physical properties [24]. One of the main parameters that affect the features of bimetallic electrocatalysts during their synthesis is the geometric effects, or in another word, the surface strain that arises from the different arrangements of surface atoms (expansion or compression) [25]. The unique structure of core and shell electrocatalyst could eliminate this strain effect to some extent [26]. The strain values of Pt/C and different M@Pt/C electrocatalysts could be estimated by plotting a relation between βcosθ and 4sinθ in Fig. 2. According to Williamson–Hall equation [27, 28]:

$$\beta \cos\theta = K\lambda/D + 4\varepsilon \sin\theta \tag{1}$$

where β is the full width at half maximum of XRD peaks, θ is the Bragg angle, K is the shape factor (0.9), λ is the X-ray wavelength, D is the crystallite size and ε is the average microstrain, straight line relations between βcosθ and 4sinθ would be obtained. The lattice strain values could be

Table 1 List of 2θ and d values of Pt/C, Cu@Pt/C, Ni@Pt/C and Co@Pt/C electrocatalysts as derived from their XRD charts

Pt/C		Cu@Pt/C		Ni@Pt/C		Co@Pt/C	
2θ/degree	d/Å	2θ/degree	d/Å	2θ/degree	d/Å	2θ/degree	d/Å
25.135	3.37629	24.742	3.59542	24.587	3.61782	24.509	3.62913
39.559	2.27026	39.759	2.26530	39.759	2.26530	39.929	2.25603
45.640	1.96176	46.373	1.95646	46.295	1.95956	46.498	1.95147
67.570	1.38861	67.925	1.37886	67.225	1.39151	67.769	1.38165

(a)

y = 0.0008x + 0.0176
R² = 0.7264

(b)

y = 0.0983x – 0.0989
R² = 0.9332

(c)

y = 0.0098x + 0.0108
R² = 0.9704

(d)

y = 0.0077x + 0.0217
R² = 0.1643

Fig. 2 Williamson–Hall plots of **a** Pt/C, **b** Cu@Pt/C, **c** Ni@Pt/C and **d** Co@Pt/C electrocatalysts

calculated using the slope values as 7.50×10^{-4}, 9.82×10^{-2}, 9.75×10^{-3} and 7.74×10^{-3} for Pt/C, Cu@Pt/C, Ni@Pt/C and Co@Pt/C electrocatalysts, respectively. This high value of lattice strain at Cu@Pt/C might account for the observed

broadening of its XRD peaks. This was also related to the large volume of grain boundaries [29]. On the other hand, Ni@Pt/C and Co@Pt/C electrocatalysts displayed lower lattice strain values among the studied ones. The lattice strain

is a result of dislocations, internal stress, grain boundaries and formation of small crystals. Therefore, lowered values would be related to increased electrocatalyst activity [30].

TEM pictures of Pt/C and different M@Pt/C electrocatalysts were described in Fig. 3. Intense and aggregated platinum nanoparticles would cover the carbon surface at Pt/C in Fig. 3a. On the other hand, defined deposits were shown for electrocatalysts containing copper (Fig. 3b) and nickel (Fig. 3c), while Co@Pt/C electrocatalyst did not display identified platinum nanoparticles, on contrary they tend to tincture the carbon support in Fig. 3d. The corresponding particle size distribution curves were constructed in Fig. 3a′–c′ by measuring the diameter of about 100 nanoparticles. A broad curve was shown by Pt/C, while the electrocatalysts containing copper or nickel exhibited shrunk platinum size range. It was difficult to build up this histogram for Co@Pt/C electrocatalyst due to its specific morphology. The most predominated Pt particle size value at Pt/C, Cu@Pt/C and Ni@Pt/C electrocatalysts were 3.5, 2 and 4 nm, respectively. The obtained Pt nanoparticles size at Cu@Pt/C was smaller than that at Pt–CeO$_2$/C (2.50 nm), Pt–ZrO$_2$/C (2.33 nm) [31] and Pt–MnO$_2$/C (2.22 nm) [32] electrocatalysts that were prepared using modified microwave-assisted polyol process. Although the dispersion of Pt/C was improved by adding TiO$_2$, the measured platinum nanoparticles diameter increased from 3.57 to 4.38 nm [31]. The elemental structure of Co@Pt/C electrocatalyst was studied using EDX analysis technique in Fig. 4a. The characteristic peaks of carbon, platinum and cobalt were observed and their relative distribution was investigated using the elemental mapping pictures in Fig. 4b–d, respectively. The atomic ratio of platinum:cobalt was measured at 0.88:1.13 that was close to the suggested nominal ratio of 1:1.

The electrochemical behavior of different M@Pt/C electrocatalysts in 0.5 M NaOH solution could be studied in Fig. 5 at 50 mVs^{-1} in relation to that of Pt/C. All cyclic voltammograms displayed three defined regions in the anodic direction; hydrogen adsorption region, platinum oxide species formation and oxygen gas evolution [33, 34]. On the other hand, this formed platinum oxide was further reduced in the backward direction at potential values extending from 55 to −630 mV. Adding transition metal to Pt/C significantly increased the area under peaks that were related to hydrogen adsorption/desorption and platinum oxide formation/reduction processes. Adding transition metal to Pt/C significantly increased the area under peaks that were related to hydrogen adsorption/desorption and platinum oxide formation/reduction processes. This could be interpreted based on the concept of the pseudocapacitive behavior of redox systems. Here, the introduced transition metals could offer increased number of adsorption sites for active species on platinum surface [35]. A strong pseudocapacitive behavior is related to the increased number of active sites at the surface of

studied electrocatalyst that can adsorb active species during the electrochemical reaction. This adsorption process can be observed within a wide range of potential values, where the adsorption energy values are not equal for all active sites. Therefore, this pseudocapacitive behavior of the studied electrocatalyst can be considered as a measure for the formed number of sufficient active sites for further alcohol oxidation reaction [36]. This sequence could be arranged in an ascending order as Pt/C < Cu@Pt/C < Ni@Pt/C ~ Co@Pt/C. The hydrogen desorption charge was taken as a measure for the electrochemical active surface area (ECSA) of studied electrocatalysts according to the equation:

$$ECSA = Q_{Hdes.}/Q_{ref} \times L_{Pt} \qquad (2)$$

where $Q_{Hdes.}$ is the required charge for the desorption of hydrogen atoms after subtracting the double layer region [33, 37], Q_{ref} is the required charge for the adsorption of one monolayer of hydrogen atoms at Pt surface [210 μC cm^{-2}] and L_{Pt} is the electrocatalyst loading in mg cm^{-2} [34, 38]. ECSA values of Pt/C, Cu@Pt/C, Ni@Pt/C and Co@Pt/C electrocatalysts were 1.44, 9.44, 13.00 and 13.89 m^2 g^{-1}.
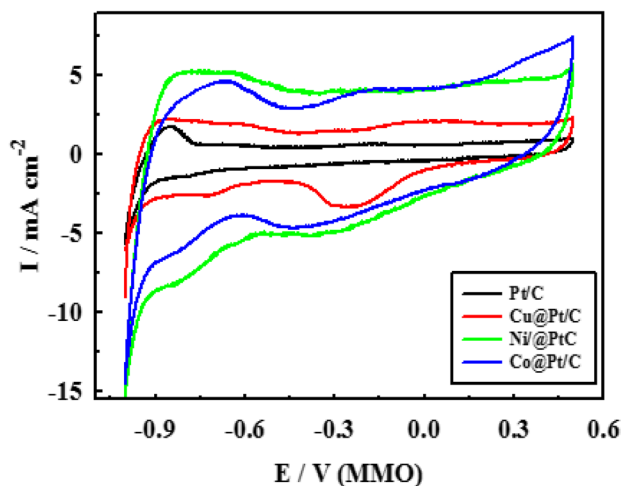
The electrocatalytic ability of Pt/C, Cu@Pt/C, Ni@Pt/C and Co@Pt/C electrocatalysts for ethanol oxidation reaction was investigated in (0.5 M ethanol + 0.5 M NaOH) solution through cyclic voltammetry technique in the potential range between −700 and +400 mV at 10 mV s^{-1} in Fig. 6. A characteristic oxidation peak for ethanol molecules was observed in all curves. After getting a maximum current density value, a continuous decay was shown as a result of the formation of incomplete oxidation products [39]. The oxidation of ethanol molecules at Cu@Pt/C, Ni@Pt/C and Co@Pt/C electrocatalysts began at −600, −600 and −554 mV, respectively as more negative onset potential values when compared to that at Pt/C (−522 mV). Accordingly, the incorporation of a transition metal with Pt could improve its CO tolerance. The oxidation current density at various electrocatalysts decreased in the order: Ni@Pt/C ≈ Co@Pt/C > Cu@Pt/C >>> Pt/C. Here, the oxidation current density at Cu@Pt/C was about 12.32 times higher than that at Pt/C. Moreover, the oxidation peak potential value was also affected by the type of added transition metal, where the most negative potential value was recorded at Cu@Pt/C (−192 mV), followed by Ni@Pt/C (−148 mV) and Co@Pt/C (−130 mV). From the above results that were summarized in Table 2, we can conclude that Co@Pt/C and Ni@Pt/C electrocatalysts showed comparable electrocatalytic performance for ethanol oxidation reaction that was generally better than that at Cu@Pt/C. Ali et al. [14] have demonstrated that the mass activity of Co@Pt/MWCNTs for alcohol oxidation was 3.36 times higher than that at Pt/C. Zhang et al. [15] have observed that supporting CoSi on graphene in Pt/CoSi-graphene could prevent the aggregation of nanosheets to get more dispersed nanoparticles with better utilization of the electrocatalyst surface. This could rationalize the improved
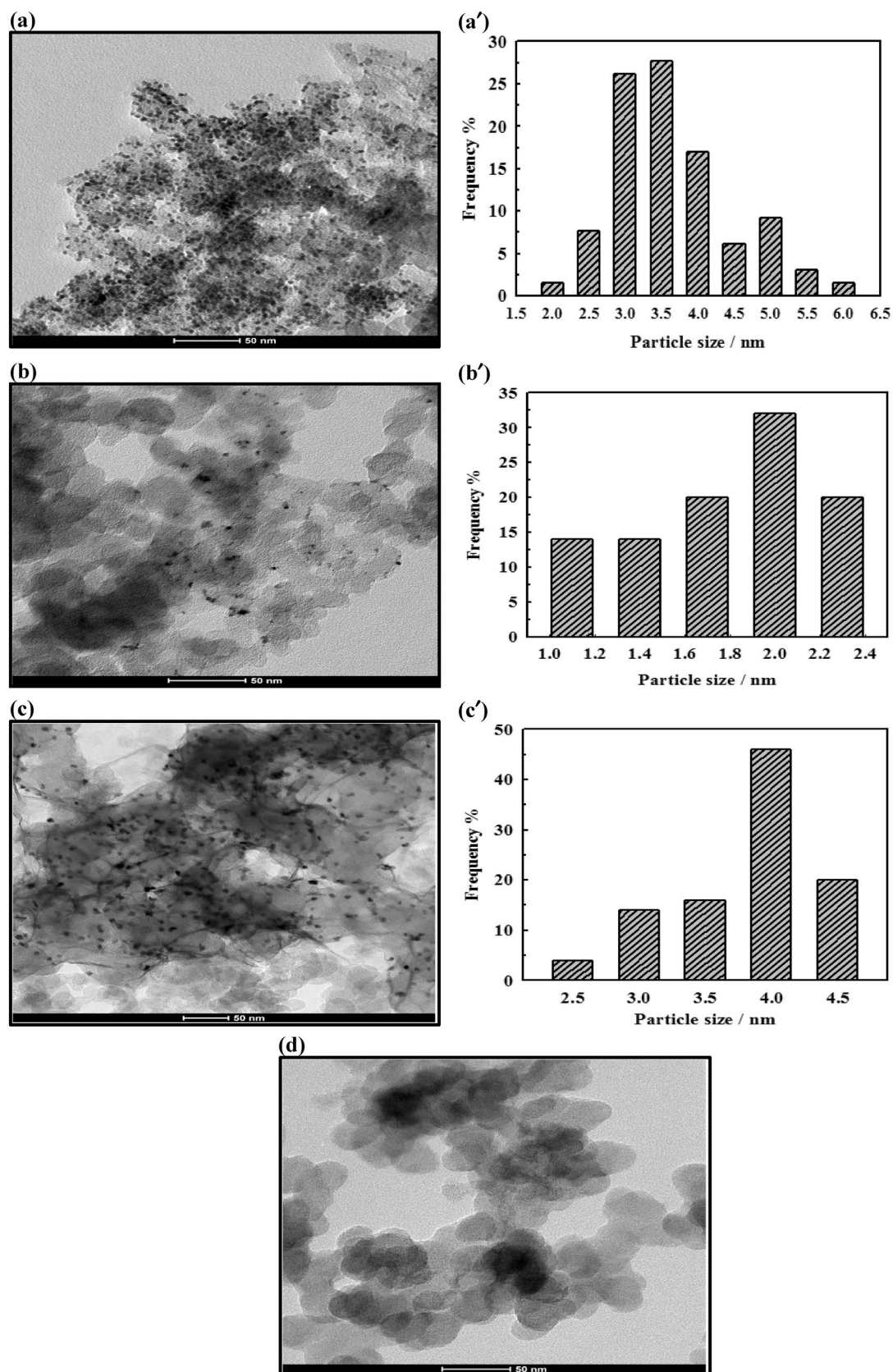
Fig. 3 TEM images of **a** Pt/C, **b** Cu@Pt/C, **c** Ni@Pt/C and **d** Co@Pt/C electrocatalysts. The respective particle size distribution curves were depicted in **a′, b′, c′**

(a)

(b) **(c)** **(d)**
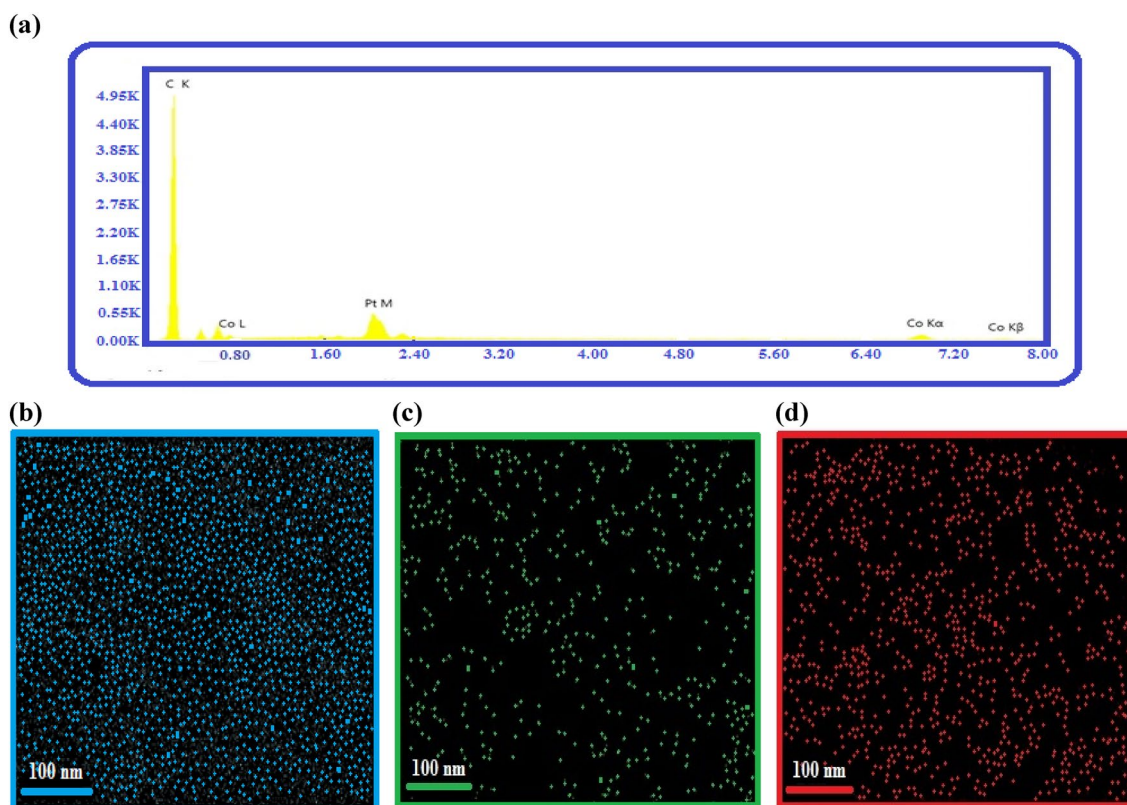
Fig. 4 **a** EDX chart of Co@Pt/C electrocatalyst and its elemental mapping pictures of **b** carbon, **c** platinum and **d** cobalt

Fig. 5 Cyclic voltammograms of Pt/C, Cu@Pt/C, Ni@Pt/C and Co@Pt/C electrocatalysts in 0.5 M NaOH solution at 50 mV s^{-1}

electrocatalytic performance of Pt/CoSi-graphene when compared to Pt/graphene. The superior electrocatalytic activity of transition metal@Pt/C electrocatalyst could be rationalized to the change in the surface electronic structure due to the lattice strain and surface ligand effects [40, 41]. This lattice mismatch between Pt shell and transition metal core could decrease the

interatomic distance in the shell to shift the d-band and reduce Pt–CO$_{ads}$ binding energy [26, 42–44]. Moreover, many surface defect sites such as step edges and kinks were formed due to the lattice compression, which in turn showed high catalytic activity for alcohol oxidation [45].

To follow the effect of ethanol concentration on the oxidation reaction at different electrocatalysts, linear sweep voltammetry was applied at various fuel concentration values in 0.5 M NaOH solution at a scan rate value of 10 mV s^{-1} in Fig. 7a–c. It was observed that the oxidation peak current density values increased with increasing ethanol concentration for all electrocatalysts. Their linear relationship in Fig. 7d suggested that the oxidation process is controlled by a diffusion mechanism. The presence of another metal (copper, nickel or cobalt) together with platinum greatly enhanced ethanol oxidation current density at all studied ethanol concentration values. The logarithmic plot of oxidation peak current density with ethanol concentration resulted in straight lines (see Fig. 7e) with slope values equal to the reaction order with respect to fuel concentration based on the relation:

$$\text{Rate } \alpha I = kC^n \tag{3}$$

$$\log I = \log k + n \log C \tag{4}$$

(a)

(b)

(c)

(d)
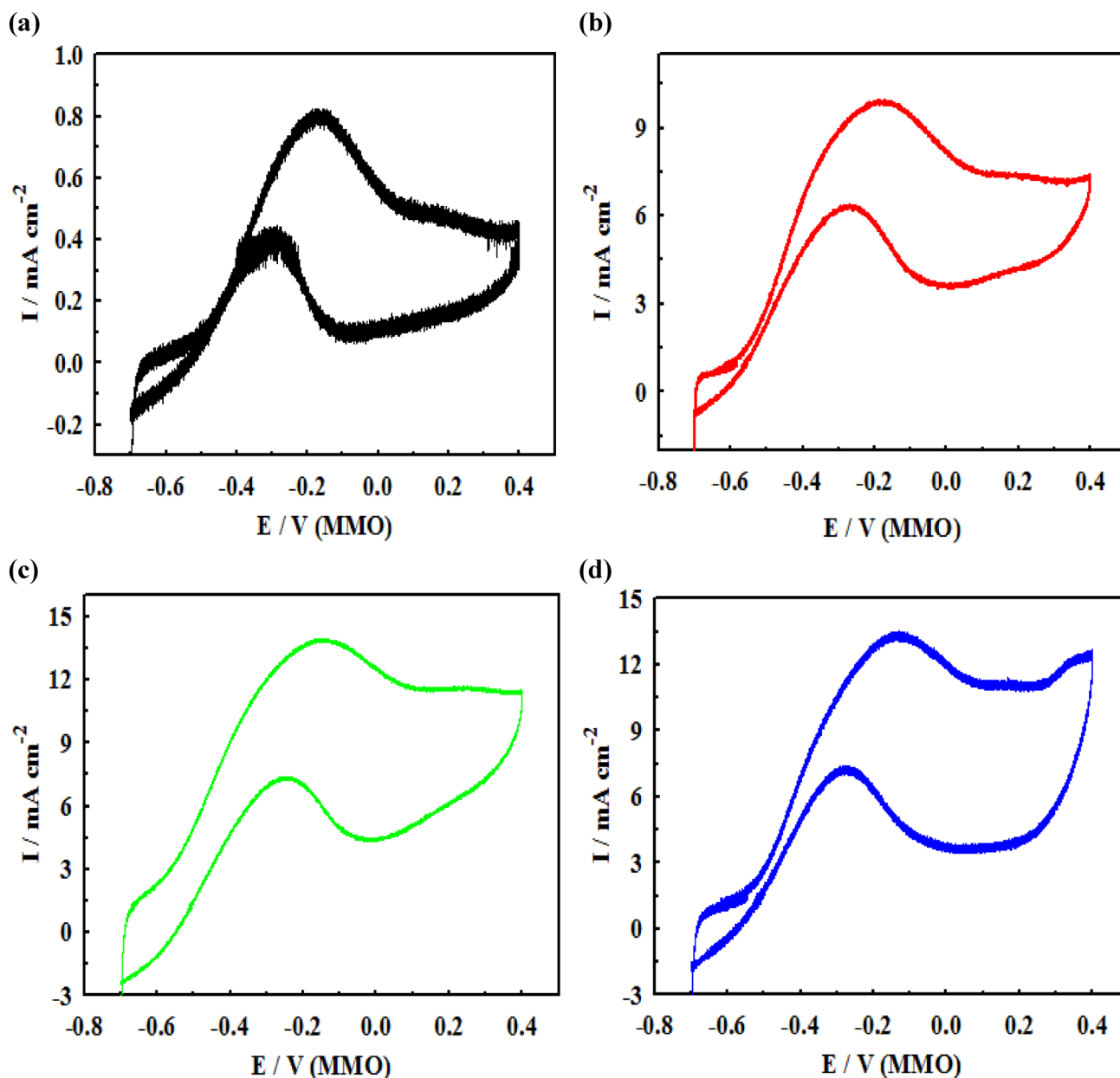
Fig. 6 Cyclic voltammograms of ethanol oxidation reaction at **a** Pt/C, **b** Cu@Pt/C, **c** Ni@Pt/C and **d** Co@Pt/C electrocatalysts in (0.5 M ethanol + 0.5 M NaOH) solution at 10 mV s^{-1}

Table 2 Electrochemical parameters of Pt/C, Cu@Pt/C, Ni@Pt/C and Co@Pt/C electrocatalysts during ethanol oxidation reaction in 0.5 M ethanol in 0.5 M NaOH solution at 10 mV s^{-1}

Electrocatalyst	E_{onset}/mV (MMO)	E_p/mV (MMO)	I/mA cm^{-2}	I_f/I_b
Pt/C	− 522	− 165	0.802	1.93
Cu@Pt/C	− 600	− 192	9.882	1.56
Ni@Pt/C	− 600	− 148	13.909	1.89
Co@Pt/C	− 554	− 130	13.390	1.85

where I is the oxidation peak current density, k is the reaction rate constant, C is ethanol concentration and n is the reaction order [46]. Values of 0.78, 0.75, 0.74 and 1.01 were calculated as the reaction order at Cu@Pt/C, Ni@Pt/C, Co@Pt/C and Pt/C electrocatalysts, respectively.

Some kinetic information on ethanol oxidation reaction at different electrocatalysts could be derived from linear sweep voltammetry technique at different scan rates. Figure 8a–c represented these curves at Cu@Pt/C, Ni@Pt/C and Co@Pt/C electrocatalysts, respectively at scan rate values of 1, 2.5, 5, 10, 20, 30, 40, 50, 75, 100, 200, 300,
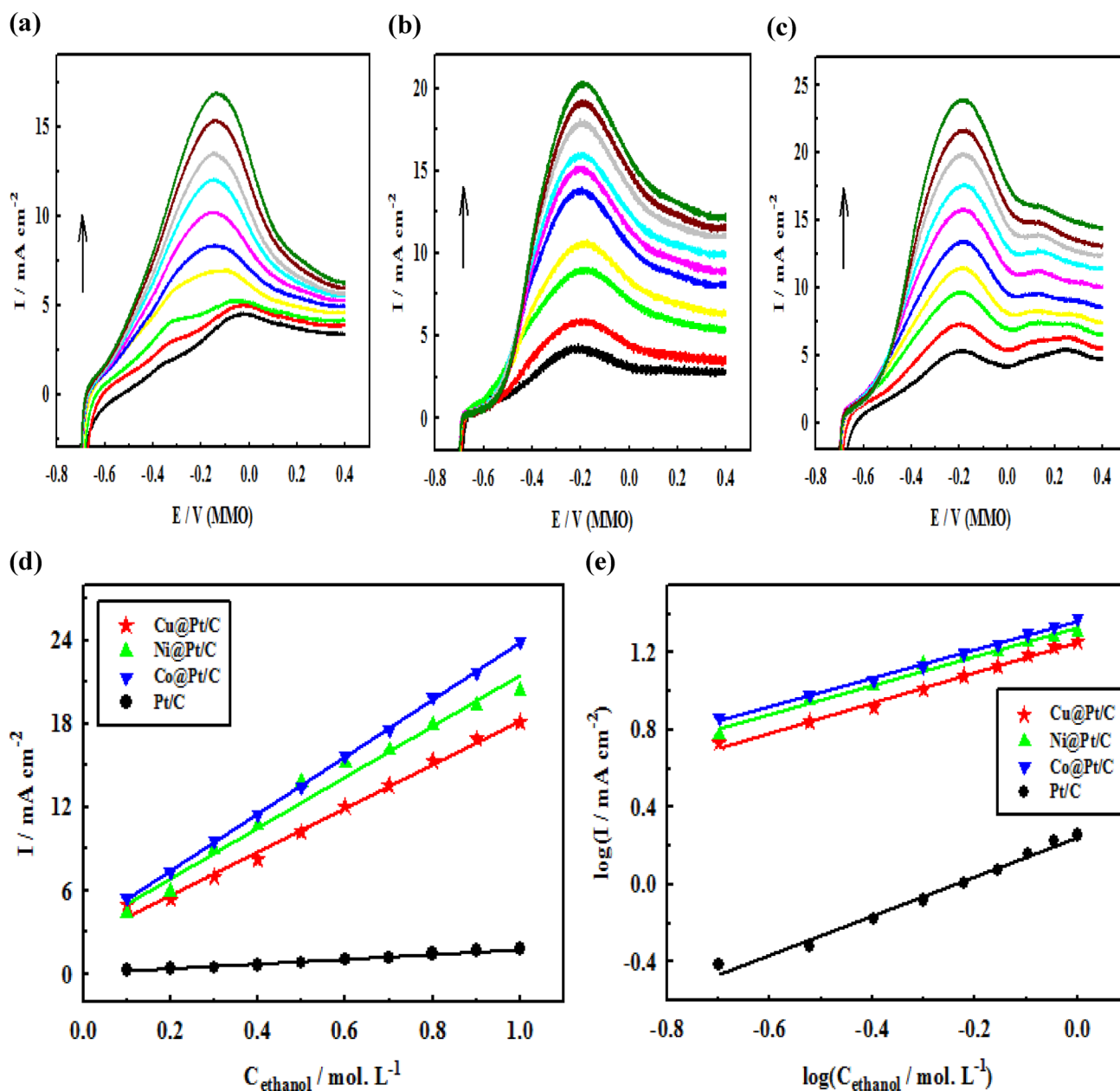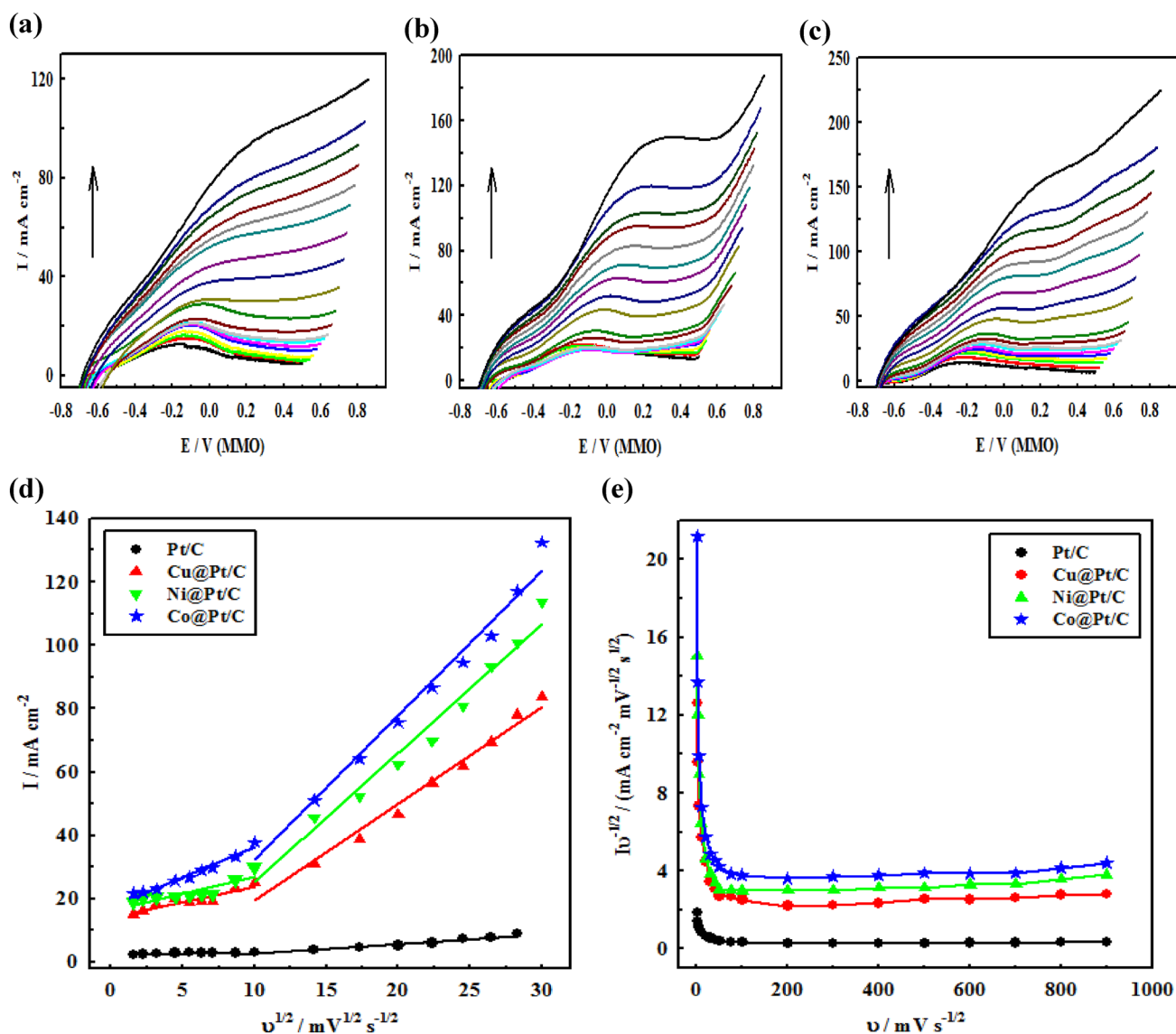
Fig. 7 Linear sweep voltammograms of ethanol oxidation at **a** Cu@Pt/C, **b** Ni@Pt/C and **c** Co@Pt/C electrocatalysts in 0.5 M NaOH solution containing various ethanol concentrations starting from 0.1 to 1 M at 10 mV s^{-1}. The variation of ethanol oxidation current density with ethanol concentration at Pt/C and different electrocatalysts is shown in **d** with their log-relationship in **e**

400, 500, 600, 700, 800, 900 and 1000 mV s^{-1} in (1 M ethanol + 0.5 M NaOH) solution. It was concluded that, as the scan rate increased, the oxidation current density increased with a shift in the potential value towards the positive direction. Linear plots were achieved when ethanol oxidation peak current density values were drawn as a function of the square root of the scan rate at all studied electrocatalysts in Fig. 8d. It corresponds to a diffusion-controlled catalytic system [47, 48]. The deviation from linear behavior at lower scan rate values in the relationship

between the oxidation peak current density and the square root of the scan rate referred to an improvement in the mass transfer step [49]. Accordingly, ethanol oxidation reaction at all electrocatalysts is kinetically controlled at low scan rate values and mass transport controlled at high scan rate values. Moreover, the relation between the scan rate-normalized current [I$\nu^{-1/2}$] and the scan rate was clarified in Fig. 8e. A non-linear relationship was obtained as a defined shape of a typical EC (electrochemical–chemical) catalytic process [50].

(a)

(b)


(c)

(d)

(e)

Fig. 8 Linear sweep voltammograms of ethanol oxidation reaction at **a** Cu@Pt/C, **b** Ni@Pt/C and **c** Co@Pt/C electrocatalysts in (1 M ethanol + 0.5 M NaOH) solution at scan rate values of 1, 2.5, 5, 10, 20, 30, 40, 50, 75, 100, 200, 300, 400, 500, 600, 700, 800, 900 and 1000 mV s^{-1}. Ethanol oxidation peak current density values with the square root of the scan rate at various electrocatalysts are shown in **d**, while **e** is the scan rate-normalized current ($I\nu^{-1/2}$) of ethanol oxidation reaction as a function of the scan rate

Tafel plots could be drawn by considering the rising part of linear sweep voltammograms of Pt/C and various M@Pt/C electrocatalysts in (1 M ethanol + 0.5 M NaOH) solution at 1 mV s^{-1}. They were demonstrated in Fig. 9. Pt/C, Cu@Pt/C, Ni@Pt/C and Co@Pt/C electrocatalysts exhibited Tafel slope values of 121.59, 229.36, 186.61 and 146.90 mV dec^{-1}, respectively to predict a similar reaction mechanism at the studied electrocatalysts. Higher Tafel slope values than 118 mV dec^{-1}, as measured here, are definite for porous electrodes with high internal surface area resulting in high electrocatalytic activity [51]. According to Butler–Volmer equation showing the relation between ethanol oxidation current density, potential and Tafel slope values [52], αn, where α is the anodic transfer coefficient and n is the number of transferred electrons, is figured out to be 0.49, 0.26, 0.32 and 0.40 for Pt/C, Cu@Pt/C, Ni@Pt/C and Co@Pt/C electrocatalysts, respectively. These low αn values led to correspondingly low α values, showing that ethanol oxidation reaction at the prepared electrocatalysts is an irreversible electrode process. By extrapolating the Tafel line, to the point where the overpotential equals zero, the exchange current density could be estimated. The exchange current density values for Cu@Pt/C, Ni@Pt/C and Co@Pt/C electrocatalysts were 1.23, 1.35 and 6.32 mA cm^{-2}, respectively. They were all higher than that for Pt/C (0.56 mA cm^{-2}) to ensure
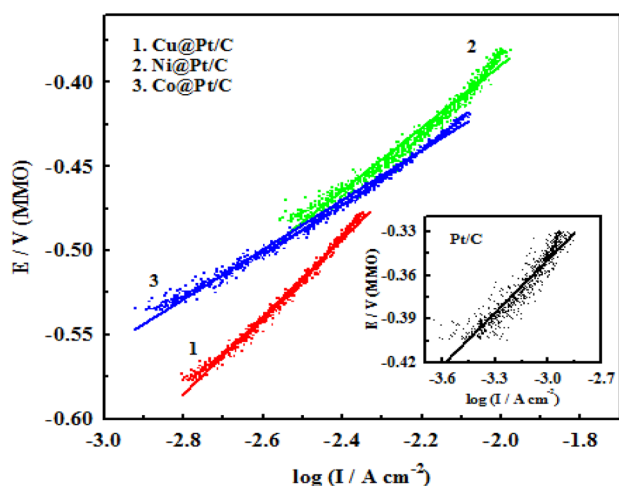
Fig. 9 Tafel plots of Pt/C, Cu@Pt/C, Ni@Pt/C and Co@Pt/C electrocatalysts in (1 M ethanol + 0.5 M NaOH) solution. They were obtained from the rising part of the corresponding linear sweep voltammograms at 1 mV s^{-1}

the enhancement of Pt/C performance by adding copper, nickel or cobalt.

The stability of synthesized electrocatalysts was investigated by chronoamperometry technique in Fig. 10. The variation of steady-state current density with time was measured in (1 M ethanol + 0.5 M NaOH) solution for 1800 s at a potential value of −200 mV (see Fig. 10a). A gradual decrease in oxidation current density was shown at all electrocatalysts before a steady-state was achieved. Generally, the activity decrease could be a result of forming an appreciable amount of poison species at platinum active sites and the transition metal oxides/hydroxides during alcohol oxidation [53]. In the steady-state region, the oxidation current density decreased in the order: Ni@Pt/C

(12.06 mA cm^{-2}) > Co@Pt/C (8.28 mA cm^{-2}) > Cu@Pt/C (1.69 mA cm^{-2}) > Pt/C (0.33 mA cm^{-2}). An appreciable enhancement in the stability performance was observed for Pt/C electrocatalyst, especially after introducing nickel or cobalt. The decay of Pt/C and M@Pt/C electrocatalysts was relatively measured at different time intervals throughout the whole chronoamperometric experiment in Fig. 10b. Adding different transition metals to Pt/C was found to significantly retard the formed electrocatalyst deactivation. By relating the obtained steady-state oxidation current density at 1800 s to that at 50 s, incorporating copper, nickel or cobalt into Pt/C structure improved its activity decay from 18.57% to 35.39%, 49.95% or 55.32%, respectively. Turnover number (TON) was applied as an estimate for the activity of a certain electrocatalyst. It could measure the number of alcohol molecules that were oxidized within a certain period of time at a certain potential value at the electrocatalyst surface containing a certain number of active sites [54]. Using the following equation, the corresponding TON values for studied electrocatalysts could be calculated:

$$\text{TON (molec. site}^{-1}\text{s}^{-1}) = j\, N_A / nF \left(1.3 \times 10^{15}\right) \qquad (5)$$
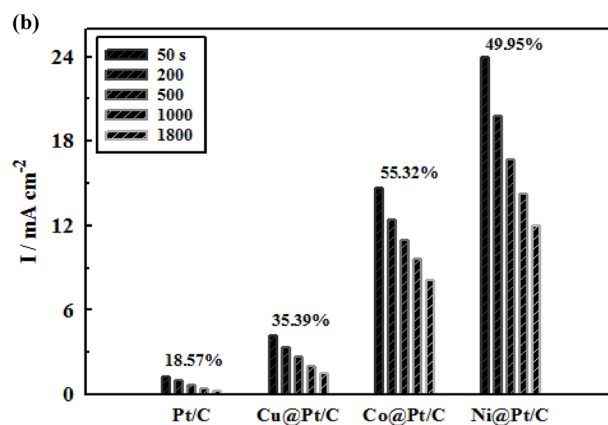
where j is the limiting current density in A cm^{-2}, N_A is Avogadro number, n is the number of obtained electrons

Table 3 TON values of Pt/C and different M@Pt/C electrocatalysts in 1 M ethanol in 0.5 M NaOH solution at a potential value of −200 mV

Electrocatalyst	TON/ molec. site^{-1} s^{-1}
Pt/C	0.171
Cu@Pt/C	0.674
Co@Pt/C	3.352
Ni@Pt/C	4.786
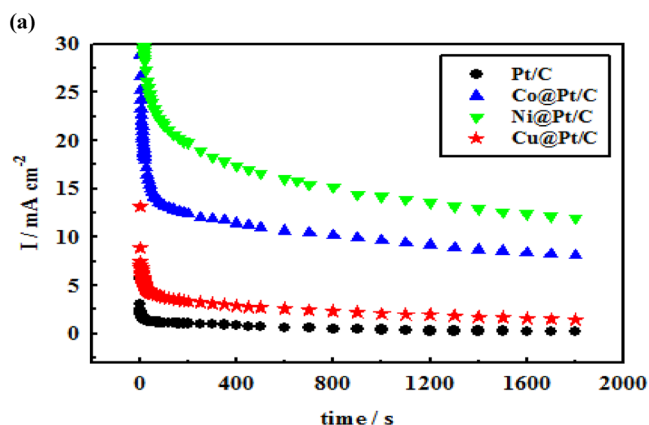
Fig. 10 a Chronoamperograms of ethanol oxidation at Pt/C, Cu@Pt/C, Co@Pt/C and Ni@Pt/C electrocatalysts in 1 M ethanol in 0.5 M NaOH solution at a potential value of −200 mV for 1800 s. **b** Vertical histogram for the relative decay of these electrocatalysts at different time intervals during the chronoamperometric study

during the oxidation of one molecule of ethanol and F is Faraday constant. Table 3 involved the calculated TON values at various M@Pt/C electrocatalysts in relation with that at Pt/C. Co@Pt/C and Ni@Pt/C electrocatalysts displayed extraordinary TON values as 19.60 and 28.00 folds higher than that at Pt/C. These TON values were also much higher than those measured at Ni@Pt/C electrocatalysts, prepared by our research group using ethylene glycol as a reducing

agent with adding different Ni:Pt atomic ratios. They demonstrated TON values ranging between 0.72 and 2.20 molec. $site^{-1}\,s^{-1}$ for electrocatalysts with varied Ni:Pt atomic ratios from 0.25:1 up to 2:1 [55].

The electrocatalytic activity of Pt/C, Cu@Pt/C, Ni@Pt/C and Co@Pt/C electrocatalysts was also examined using electrochemical impedance spectroscopy. The corresponding phase shift diagrams were inserted in Fig. 11a in
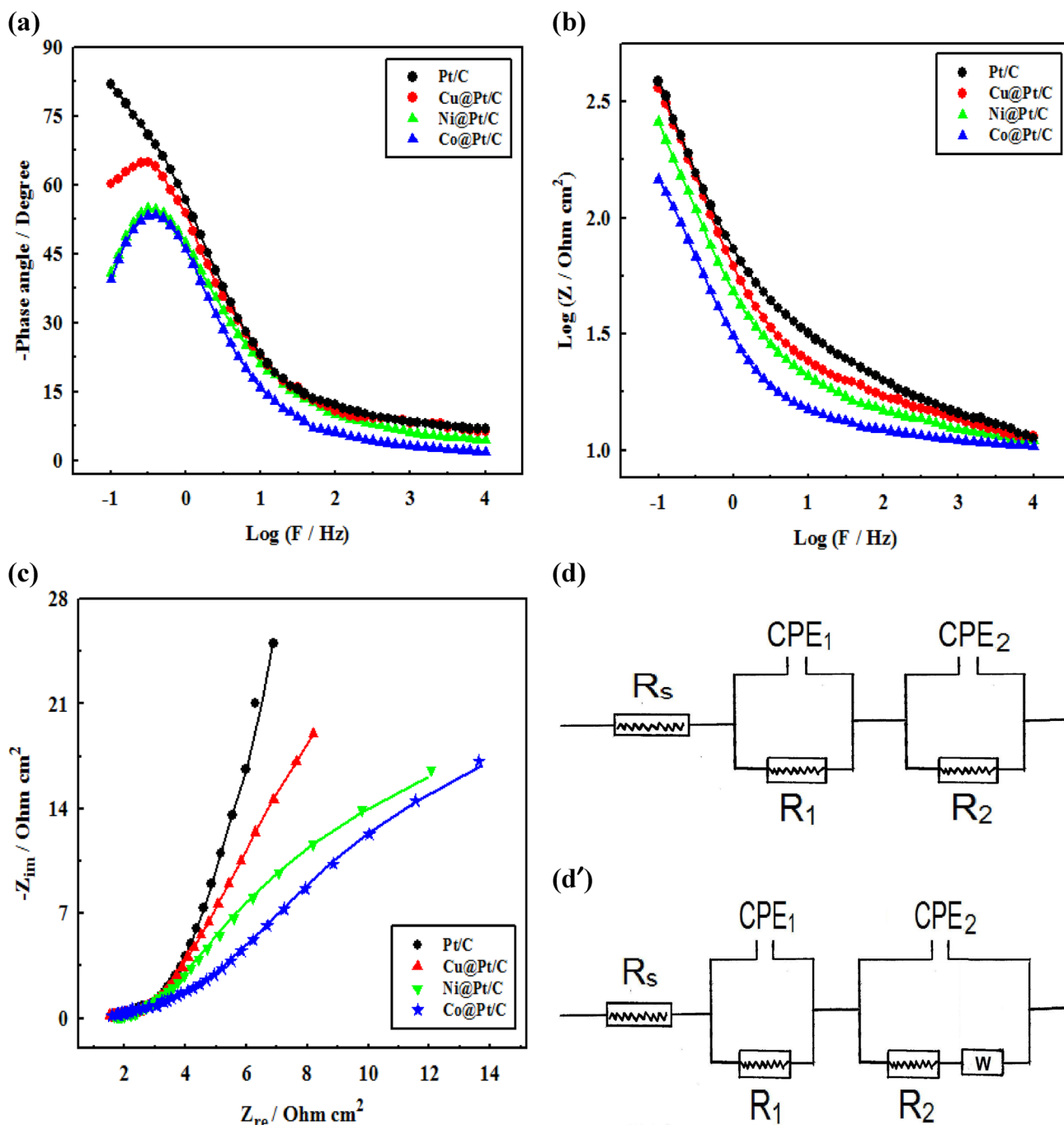
Fig. 11 **a, b** Bode and **c** Nyquist plots of Pt/C, Cu@Pt/C, Ni@Pt/C and Co@Pt/C electrocatalysts in 1 M ethanol in 0.5 M NaOH solution at a potential value of -450 mV in the frequency range of 1×10^4–0.1 Hz. **d, d′** The proposed equivalent electric circuit models

Table 4 List of electrochemical parameters of impedance study for ethanol oxidation at Pt/C and different M@Pt/C electrocatalysts in 0.5 M NaOH solution containing 1 M ethanol at a potential value of −450 mV in the frequency range of 1×10^4–0.1 Hz

Electrocatalyst	R_s/Ohm	Y_1/ Ohm^{-1} s^a cm^{-2}×10^{-3}	a_1	R_1/Ohm cm^2	Y_2/Ohm^{-1} s^a cm^{-2}×10^{-3}	a_2	R_2/Ohm cm^2	W/kOhm s$^{-1/2}$ cm^2	B/s$^{1/2}$
Pt/C	2.55	217.86	0.920	3.00	3.77	0.120	183.10	1.54	0.823
Cu@Pt/C	2.55	147.71	0.960	3.06	26.41	0.168	90.31	–	–
Ni@Pt/C	3.41	69.29	0.997	3.56	40.16	0.345	50.63	–	–
Co@Pt/C	2.64	30.16	1.000	5.02	44.80	0.355	40.45	–	–

Table 5 List of electrochemical parameters of previously studied Pt-based electrocatalysts during ethanol oxidation reaction

Electrocatalyst	Tested solution	Scan rate/ mV s^{-1}	E_{onset}/mV (MMO)	E_P/mV (MMO)	I_p	I_L	ECSA/ m^2 g^{-1}	I_f/I_b	References
Pt/C	1 M ethanol + 0.5 M NaOH	50	−480	172	37.8 mA cm^{-2}	5.1 mA cm^{-2}	25.10	2.37	[56]
Pt/NGs[a]	1 M ethanol + 0.5 M NaOH	50	−340	80	45.0 mA cm^{-2}	6.2 mA cm^{-2}	33.90	8.72	[56]
AuPt/C	1 M ethanol + 0.5 M NaOH	50	−470	243	58.0 mA cm^{-2}	13.3 mA cm^{-2}	43.60	5.80	[56]
AuPt/NGs[a]	1 M ethanol + 0.5 M NaOH	50	−590	161	83.2 mA cm^{-2}	18.2 mA cm^{-2}	57.10	–	[56]
AuPt/NGs–PVP[b]	1 M ethanol + 0.5 M NaOH	50	−635	126	120.0 mA cm^{-2}	26.8 mA cm^{-2}	78.90	6.10	[56]
Pt/PNVC–V$_2$O$_5$[c]	1 M ethanol + 0.5 M NaOH	50	−580	250	62.0 mA cm^{-2}	–	31.30	7.75	[57]
PtPd/PNVC–V$_2$O$_5$[c]	1 M ethanol + 0.5 M NaOH	50	−630	375	97.8 mA cm^{-2}	–	54.30	2.49	[57]
Ni$_1$Pt$_1$/DNA-rGO[d]	1 M ethanol + 0.5 M KOH	50	−405	−150	0.54 A mg$^{-1}_{metal}$	–	33.87	2.70	[58]
Pd$_1$Pt$_1$/DNA–rGO[d]	1 M ethanol + 0.5 M KOH	50	−410	30	1.18 A mg$^{-1}_{metal}$	–	44.14	1.07	[58]
Ni$_1$Pd$_1$Pt$_1$/DNA–rGO[d]	1 M ethanol + 0.5 M KOH	50	−460	30	3.40 A mg$^{-1}_{metal}$	–	68.57	1.21	[58]
Pt/C	1 M ethanol + 1 M KOH	10	−467	−24	23 A g$^{-1}_{Pt}$	1.5 A g$^{-1}_{Pt}$	–	–	[59]
PtBi/C (90:10)	1 M ethanol + 1 M KOH	10	−491	101	33 A g$^{-1}_{Pt}$	7.7 A g$^{-1}_{Pt}$	–	–	[59]
PtBi/C (70:30)	1 M ethanol + 1 M KOH	10	−501	66	45 A g$^{-1}_{Pt}$	10.2 A g$^{-1}_{Pt}$	–	–	[59]
PtBi/C (50:50)	1 M ethanol + 1 M KOH	10	−511	89	64 A g$^{-1}_{Pt}$	12.0 A g$^{-1}_{Pt}$	–	–	[59]

[a]*NGs* graphene sheets

[b]*NGs-PVP* graphene sheets stabilized with polyvinylpyrrolidone

[c]*PNVC–V$_2$O$_5$* poly-vinyl carbazole (PNVC) cross-linked with V$_2$O$_5$

[d]*DNA-rGO* deoxyribonucleic acid-modified reduced graphene oxide

(1 M ethanol + 0.5 M NaOH) solution at a potential value of −450 mV in the frequency range from 1×10^4 to 0.1 Hz. The phase angle value slightly increased for all electrocatalysts with decreasing the frequency value down to 47.75 Hz. Therefore, a resistive behavior was noticed with low electrocatalytic activity within this frequency region. At lower frequency values, a capacitive behavior was observed at Cu@ Pt/C, Ni@Pt/C and Co@Pt/C electrocatalysts with a maximum phase angle at a certain frequency value. This maximum of −θ value showed its highest value in Cu@Pt/C electrocatalyst, while Ni@Pt/C and Co@Pt/C have almost equal decreased phase angle at this maximum value. Pt/C almost displayed an inclined line in this low-frequency region. Moreover, the dependence of log Z on log F was shown in

Fig. 11b. The impedance value generally decreased in the order: Pt/C > Cu@Pt/C > Ni@Pt/C > Co@Pt/C. Generally, a gradual increase in the impedance value was observed with shifting towards lower frequency values, followed by sharp increase up to 0.1 Hz. The corresponding Nyquist plots of these electrocatalysts were shown in Fig. 11c. Two overlapping capacitive semicircles were observed in high and low-frequency regions in all M@Pt/C electrocatalysts. However, Pt/C exhibited a linear behavior in the low-frequency region. An equivalent electric circuit was described in Fig. 11d. Here, the solution resistance (R_s) is connected in series to two (R–CPE) networks. CPE could represent the constant phase element that fits the porous electrocatalyst surface. The resistance values of the outer and inner layers could be expressed by R_1 and R_2, respectively. An extra electric element was added in series to R_2 in Fig. 11d′. It is a Warburg impedance element that could describe the linear region in the Nyquist plot of Pt/C. The estimated electrochemical impedance parameters were summarized in Table 4. All electrocatalysts containing transition metals demonstrated reduced charge transfer resistance (R_2) values in relation to that at Pt/C. This could be deduced from their lowered diameter of the semicircle in low-frequency region. This observation could support the improved performance of formed electrocatalysts after introducing either copper or nickel or cobalt in the core structure of Pt/C.

Our obtained results for ethanol electro-oxidation at M@Pt/C electrocatalysts were compared with those at previously reported electrocatalysts in the literature [56–59]. More negative E_{onset} and E_p values were measured at our M@Pt/C electrocatalysts in relation to those at the listed electrocatalysts in Table 5. Generally, the outperformed behavior of M@Pt/C electrocatalysts towards ethanol oxidation reaction was rationalized to the adsorption of OH species at the transition metal surface rather than on platinum at lower potential values, thus enhancing the removal of accumulated CO molecules through their oxidation into CO_2 [60, 61]. Furthermore, the change of bond distance inside platinum crystal lattice in M@Pt/C electrocatalysts could also alter their electronic properties that in turn retarded the adsorption of poisoning species [62]. The increased ECSA values of M@Pt/C electrocatalysts, especially those containing nickel (13.00 m^2 g^{-1}) and cobalt (13.89 m^2 g^{-1}) could reflect the availability of more active sites at their surfaces for adsorbing alcohol molecules for further electro-oxidation.

4 Conclusion

Different transition metals were incorporated in the core structure of Pt/C with the application of $NaBH_4$ during the reduction step and examined as electrocatalysts for ethanol oxidation in alkaline medium. ECSA measurements indicated the formation of an increased number of platinum active sites at M@Pt/C in relation to that at Pt/C. Introducing copper or nickel in the electrocatalyst structure resulted in decreased onset potential values during ethanol oxidation reaction. A superior exchange current density value was obtained at Co@Pt/C supporting its improved catalytic activity. Moreover, the relative decay of electrochemical performance of various M@Pt/C electrocatalysts during the stability test exhibited increased resistance for CO molecules accumulation. The addition of copper, nickel or cobalt to Pt/C could also enhance the charge transfer resistance at its surface in ethanol oxidation process as inferred by electrochemical impedance experiments.

References

1. A.A. El-Shafei, Electrocatalytic oxidation of methanol at a nickel hydroxide/glassy carbon modified electrode in alkaline medium. J. Electroanal. Chem. **471**(2), 89–95 (1999)
2. C. Lamy, J.-M. Léger, S. Srinivasan, Direct methanol fuel cells: from a twentieth century electrochemist's dream to a twenty-first century emerging technology, in *Modern Aspects of Electrochemistry*, ed. by J.O. Bockris (Kluwer Academic, New York, 2001), pp. 53–118
3. J. van Drunen, T.W. Napporn, B. Kokoh, G. Jerkiewicz, Electrochemical oxidation of isopropanol using a nickel foam electrode. J. Electroanal. Chem. **716**, 120–128 (2014)
4. J.P. Pereira, D.S. Falcão, V.B. Oliveira, A.M.F.R. Pinto, Performance of a passive direct ethanol fuel cell. J. Power Sources **256**, 14–19 (2014)
5. E. Antolini, Catalysts for direct ethanol fuel cells. J. Power Sources **170**(1), 1–12 (2007)
6. C. Hu, H. Cheng, Y. Zhao, Y. Hu, Y. Liu, L. Dai, L. Qu, Newly-designed complex ternary Pt/PdCu nanoboxes anchored on three-dimensional graphene framework for highly efficient ethanol oxidation. Adv. Mater. **24**(40), 5493–5498 (2012)
7. E. Higuchi, T. Takase, M. Chiku, H. Inoue, Preparation of ternary $Pt/Rh/SnO_2$ anode catalysts for use in direct ethanol fuel cells and their electrocatalytic activity for ethanol oxidation reaction. J. Power Sources **263**, 280–287 (2014)
8. A.O. Neto, L.A. Farias, R.R. Dias, M. Brandalise, M. Linardi, E.V. Spinacé, Enhanced electro-oxidation of ethanol using $PtSn/CeO_2$–C electrocatalyst prepared by an alcohol-reduction process. Electrochem. Commun. **10**(9), 1315–1317 (2008)
9. J. Seweryn, A. Lewera, High selectivity of ethanol electrooxidation to carbon dioxide on platinum nanoparticles in low temperature polymer electrolyte membrane direct ethanol fuel cell. Appl. Catal. B **144**, 129–134 (2014)
10. Z. Yan, H. Wang, M. Zhang, Z. Jiang, T. Jiang, J. Xie, Pt supported on Mo_2C particles with synergistic effect and strong interaction force for methanol electro-oxidation. Electrochim. Acta **95**, 218–224 (2013)
11. Q. Jiang, L. Jiang, S. Wang, J. Qi, G. Sun, A highly active PtNi/C electrocatalyst for methanol electrooxidation in alkaline media. Catal. Commun. **12**(1), 67–70 (2010)
12. L. Tamašauskaité-Tamašiūnaité, A. Balčiūnaité, A. Vaiciukevičiené, A. Selskis, V. Pakštas, Investigation of nanostructured platinum–nickel supported on the titanium surface

as electrocatalysts for alkaline fuel cells. J. Power Sources **208**, 242–247 (2012)

13. K. Ding, Y. Zhao, L. Liu, Y. Cao, Q. Wang, H. Gu, X. Yan, Z. Guo, Pt–Ni bimetallic composite nanocatalysts prepared by using multi-walled carbon nanotubes as reductants for ethanol oxidation reaction. Int. J. Hydrog. Energy **39**(31), 17622–17633 (2014)

14. S. Ali, R. Ahmed, M. Sohail, S.A. Khan, M.S. Ansari, Co@Pt core–shell nanoparticles supported on carbon nanotubes as promising catalyst for methanol electro-oxidation. J. Ind. Eng. Chem. **28**, 344–350 (2015)

15. M. Zhang, Z. Yan, Y. Li, J. Jing, J. Xie, Preparation of cobalt silicide on graphene as Pt electrocatalyst supports for highly efficient and stable methanol oxidation in acidic media. Electrochim. Acta **161**, 48–54 (2015)

16. Q. Sheng, H. Mei, H. Wu, X. Zhang, S. Wang, A highly sensitive non-enzymatic glucose sensor based on Pt_xCo_{1-x}/C nanostructured composites. Sens. Actuators B **207**(Part A), 51–58 (2015)

17. J.M. Sieben, V. Comignani, A.E. Alvarez, M.M.E. Duarte, Synthesis and characterization of Cu core Pt–Ru shell nanoparticles for the electrooxidation of alcohols. Int. J. Hydrog. Energy **39**(16), 8667–8674 (2014)

18. A. Sarkar, A. Manthiram, Synthesis of Pt@Cu core-shell nanoparticles by galvanic displacement of Cu by Pt^{4+} ions and their application as electrocatalysts for oxygen reduction reaction in fuel cells. J. Phys. Chem. C **114**(10), 4725–4732 (2010)

19. H. Zhu, X. Li, F. Wang, Synthesis and characterization of Cu@Pt/C core-shell structured catalysts for proton exchange membrane fuel cell. Int. J. Hydrog. Energy **36**(15), 9151–9154 (2011)

20. M. Wang, Y. He, R. Li, Z. Ma, Z. Zhang, X. Wang, Electrochemical activated PtAuCu alloy nanoparticle catalysts for formic acid, methanol and ethanol electro-oxidation. Electrochim. Acta **178**, 259–269 (2015)

21. J.-I. Park, M.G. Kim, Y.-W. Jun, J.S. Lee, W.R. Lee, J. Cheon, Characterization of superparamagnetic "Core–Shell" nanoparticles and monitoring their anisotropic phase transition to ferromagnetic "solid solution" nanoalloys. J. Am. Chem. Soc. **126**(29), 9072–9078 (2004)

22. N. Kristian, X. Wang, Pt_{shell}–Au_{core}/C electrocatalyst with a controlled shell thickness and improved Pt utilization for fuel cell reactions. Electrochem. Commun. **10**(1), 12–15 (2008)

23. M. Ammam, E.B. Easton, PtCu/C and Pt(Cu)/C catalysts: synthesis, characterization and catalytic activity towards ethanol electrooxidation. J. Power Sources **222**, 79–87 (2013)

24. G. Ertl, H. Knözinger, J. Weitkamp. *Handbook of Heterogeneous Catalysis*, (Wiley, Hoboken, 2008)

25. M. Mavrikakis, B. Hammer, J.K. Nørskov, Effect of strain on the reactivity of metal surfaces. Phys. Rev. Lett. **81**(13), 2819–2822 (1998)

26. P. Strasser, S. Koh, T. Anniyev, J. Greeley, K. More, C. Yu, Z. Liu, S. Kaya, D. Nordlund, H. Ogasawara, M.F. Toney, A. Nilsson, Lattice-strain control of the activity in dealloyed core–shell fuel cell catalysts. Nat. Chem. **2**, 454–460 (2010)

27. S. Kumar, S. Supriya, L.K. Pradhan, M. Kar, Effect of microstructure on electrical properties of Li and Cr substituted nickel oxide. J. Mater. Sci. **28**(22), 16679–16688 (2017)

28. A.A. Sattar, H.M. El-Sayed, K.M. El-Shokrofy, M.M. El-Tabey, Study of the dc resistivity and thermoelectric power in Mn-substituted Ni–Zn ferrites. J. Mater. Sci. **42**(1), 149–155 (2007)

29. W. Dmowski, T. Egami, K.E. Swider-Lyons, C.T. Love, D.R. Rolison, Local atomic structure and conduction mechanism of nanocrystalline hydrous RuO_2 from X-ray scattering. J. Phys. Chem. B **106**(49), 12677–12683 (2002)

30. T. Ungár, Microstructural parameters from X-ray diffraction peak broadening. Scripta Mater. **51**(8), 777–781 (2004)

31. R.M. Abdel Hameed, R.S. Amin, K.M. El-Khatib, A.E. Fetohi, Influence of metal oxides on platinum activity towards methanol

oxidation in H_2SO_4 solution. ChemPhysChem **17**(7), 1054–1061 (2016)

32. R.M. Abdel Hameed, A.E. Fetohi, R.S. Amin, K.M. El-Khatib, Promotion effect of manganese oxide on the electrocatalytic activity of Pt/C for methanol oxidation in acid medium. Appl. Surf. Sci. **359**, 651–663 (2015)

33. J. Wang, D.F. Thomas, A. Chen, Nonenzymatic electrochemical glucose sensor based on nanoporous PtPb networks. Anal. Chem. **80**(4), 997–1004 (2008)

34. H. Gao, F. Xiao, C.B. Ching, H. Duan, One-step electrochemical synthesis of PtNi nanoparticle-graphene nanocomposites for nonenzymatic amperometric glucose detection. ACS Appl. Mater. Interfaces **3**(8), 3049–3057 (2011)

35. B.E. Conway, E. Gileadi, Kinetic theory of pseudo-capacitance and electrode reactions at appreciable surface coverage. Trans. Faraday Soc. **58**, 2493–2509 (1962)

36. A. Eftekhari, From pseudocapacitive redox to intermediary adsorption in oxygen evolution reaction. Mater. Today Chem. **4**, 117–132 (2017)

37. B. Lim, M. Jiang, P.H.C. Camargo, E.C. Cho, J. Tao, X. Lu, Y. Zhu, Y. Xia, Pd–Pt bimetallic nanodendrites with high activity for oxygen reduction. Science **324**(5932), 1302–1305 (2009)

38. L.-Q. Rong, C. Yang, Q.-Y. Qian, X.-H. Xia, Study of the nonenzymatic glucose sensor based on highly dispersed Pt nanoparticles supported on carbon nanotubes. Talanta **72**(2), 819–824 (2007)

39. J.M. Sieben, M.M.E. Duarte, Methanol, ethanol and ethylene glycol electro-oxidation at Pt and Pt–Ru catalysts electrodeposited over oxidized carbon nanotubes. Int. J. Hydrog. Energy **37**(13), 9941–9947 (2012)

40. V.R. Stamenkovic, B.S. Mun, K.J.J. Mayrhofer, P.N. Ross, N.M. Markovic, Effect of surface composition on electronic structure, stability, and electrocatalytic properties of Pt-transition metal alloys: Pt-skin versus Pt-skeleton surfaces. J. Am. Chem. Soc. **128**(27), 8813–8819 (2006)

41. D. Wang, H.L. Xin, H. Wang, Y. Yu, E. Rus, D.A. Muller, F.J. Disalvo, H.D. Abruňa, Facile synthesis of carbon-supported Pd–Co core-shell nanoparticles as oxygen reduction electrocatalysts and their enhanced activity and stability with monolayer Pt decoration. Chem. Mater. **24**(12), 2274–2281 (2012)

42. D. Wang, H.L. Xin, Y. Yu, H. Wang, E. Rus, D.A. Muller, H.D. Abruňa, Pt-decorated PdCo@Pd/C core-shell nanoparticles with enhanced stability and electrocatalytic activity for the oxygen reduction reaction. J. Am. Chem. Soc. **132**(50), 17664–17666 (2010)

43. A.U. Nilekar, S. Alayoglu, B. Eichhorn, M. Mavrikakis, Preferential CO oxidation in hydrogen: reactivity of core–shell nanoparticles. J. Am. Chem. Soc. **132**(21), 7418–7428 (2010)

44. C. Koenigsmann, A.C. Santulli, K. Gong, M.B. Vukmirovic, W.-P. Zhou, E. Sutter, S.S. Wong, R.R. Adzic, Enhanced electrocatalytic performance of processed, ultrathin, supported Pd–Pt core–shell nanowire catalysts for the oxygen reduction reaction. J. Am. Chem. Soc. **133**(25), 9783–9795 (2011)

45. E.R. Savinova, F. Hahn, N. Alonso-Vante, The assessment of nanocrystalline surface defects on real versus model catalysts probed via vibrational spectroscopy of adsorbed CO. Surf. Sci. **603**(10–12), 1892–1899 (2009)

46. B. Habibi, S. Ghaderi, Synthesis, characterization and electrocatalytic activity of Co@Pt nanoparticles supported on carbon-ceramic substrate for fuel cell applications. Int. J. Hydrog. Energy **40**(15), 5115–5125 (2015)

47. K. Honda, M. Yoshimura, T.N. Rao, D.A. Tryk, A. Fujishima, K. Yasui, Y. Sakamoto, K. Nishio, H. Masuda, Electrochemical properties of Pt-modified nano-honeycomb diamond electrodes. J. Electroanal. Chem. **514**(1–2), 35–50 (2001)

48. Z.-P. Sun, X.-G. Zhang, Y.-Y. Liang, H.-L. Li, Highly dispersed Pd nanoparticles on covalent functional MWNT surfaces for

methanol oxidation in alkaline solution. Electrochem. Commun. **11**(3), 557–561 (2009)

49. Z. Yan, G. He, G. Zhang, H. Meng, P.K. Shen, Pd nanoparticles supported on ultrahigh surface area honeycomb-like carbon for alcohol electrooxidation. Int. J. Hydrog. Energy **35**(8), 3263–3269 (2010)

50. R.S. Nicholson, I. Shain, Theory of stationary electrode polarography. Single scan and cyclic methods applied to reversible, irreversible, and kinetic systems. Anal. Chem. **36**(4), 706–723 (1964)

51. J.N. Soderberg, A.C. Co, A.H.C. Sirk, V.I. Birss, Impact of porous electrode properties on the electrochemical transfer coefficient. J. Phys. Chem. B **110**(21), 10401–10410 (2006)

52. A.J. Bard, L.R. Faulkner, *Electrochemical Methods—Fundamentals and Applications* (Wiley, New York, 2001)

53. E.A. Franceschini, M.M. Bruno, F.J. Williams, F.A. Viva, H.R. Corti, High-activity mesoporous Pt/Ru catalysts for methanol oxidation. ACS Appl. Mater. Interfaces **5**(21), 10437–10444 (2013)

54. A. Wieckowski, *Interfacial Electrochemistry: Theory, Experiment and Applications* (Marcel Dekker, New York, 1999), p. 950

55. A.E. Fetohi, R.S. Amin, R.M. Abdel Hameed, K.M. El-Khatib, Effect of nickel loading in Ni@Pt/C electrocatalysts on their activity for ethanol oxidation in alkaline medium. Electrochim. Acta **242**, 187–201 (2017)

56. A. Dutta, J. Ouyang, Enhanced electrocatalytic performance on polymer-stabilized graphene decorated with alloy nanoparticles for ethanol oxidation reaction in alkaline media. Appl. Catal. B **158–159**, 119–128 (2014)

57. J. Datta, A. Dutta, M. Biswas, Enhancement of functional properties of PtPd nano catalyst in metal-polymer composite matrix: application in direct ethanol fuel cell. Electrochem. Commun. **20**, 56–59 (2012)

58. J. Ma, J. Wang, G. Zhang, X. Fan, G. Zhang, F. Zhang, Y. Li, Deoxyribonucleic acid-directed growth of well dispersed nickel–palladium–platinum nanoclusters on graphene as an efficient catalyst for ethanol electrooxidation. J. Power Sources **278**, 43–49 (2015)

59. M.M. Tusi, N.S.O. Polanco, S.G. da Silva, E.V. Spinacé, A.O. Neto, The high activity of PtBi/C electrocatalysts for ethanol electro-oxidation in alkaline medium. Electrochem. Commun. **13**(2), 143–146 (2011)

60. W. Zhou, Z. Zhou, S. Song, W. Li, G. Sun, P. Tsiakaras, Q. Xin, Pt based anode catalysts for direct ethanol fuel cells. Appl. Catal. B **46**(2), 273–285 (2003)

61. P.E. Tsiakaras, PtM/C (M = Sn, Ru, Pd, W) based anode direct ethanol–PEMFCs: Structural characteristics and cell performance. J. Power Sources **171**(1), 107–112 (2007)

62. L. Zhang, D. Xia, Electrocatalytic activity of ordered intermetallic PtSb for methanol electro-oxidation. Appl. Surf. Sci. **252**(6), 2191–2195 (2006)